Ligand–metal synergy in MOF-derived Co–Ni(TCNQ)$_2$·2H$_2$O for efficient HMF electrooxidation and hydrogen Co-production

Ting Xiang[a,b], Njud S. Alharbi[c], Xijun Wang*[a,d], Changlun Chen*[b]

[a] *University of Science and Technology of China, Hefei 230026, PR China*

[b] *Institute of Plasma Physics, HFIPS, Chinese Academy of Sciences, Hefei 230031, PR China.*

[c] *Department of Biological Sciences, Faculty of Science, King Abdulaziz University, Jeddah 21589, Saudi Arabian*

[d]*State Key Laboratory of Precision and Intelligent Chemistry, University of Science and Technology of China, Hefei, Anhui 230026, China*

* Corresponding author: xijun@ustc.edu.cn (X. J. Wang), clchen@ipp.ac.cn (C.L. Chen)

Density functional theory calculations (DFT)

The initial unit cell models for the monometallic and bimetallic systems were constructed based on the reported $Mn(TCNQ)_2(H_2O)_2$ framework (CCDC No. 1225268), in which the Mn(II) centers were substituted by Co(II) and/or Ni(II) ions.

The adsorption energies (E_{ads}) were calculated using the following equation:

$$E_{ads} = E_{model+sub} - E_{model} - E_{sub}$$

where $E_{model+sub}$, E_{model}, and E_{sub} represent the total energies of the adsorption configuration, the clean model, and the isolated adsorbate molecule, respectively.

The HMF oxidation reaction (HMFOR) was modeled through the following sequence of elementary steps:

$$*+ HMF \rightarrow *HMF$$

$$*HMF - e^- + OH^- \rightarrow *HMF - H + H_2O$$

$$*HMF - H - e^- + OH^- \rightarrow *HMFCA$$

$$*HMFCA - e^- + OH^- \rightarrow *HMFCA - H + H_2O$$

$$*HMFCA - H - e^- + OH^- \rightarrow *FFCA + H_2O$$

$$*FFCA - e^- + OH^- \rightarrow *FFCA - H + H_2O$$

$$*FFCA - H - e^- + OH^- \rightarrow *FDCA$$

$$*FDCA \rightarrow *+ FDCA$$

where * denotes the active site on the catalyst surface.

The computational hydrogen electrode (CHE) model was employed to evaluate the effect of applied potential on each electrochemical step [1]. For every electron-transfer reaction, the free energy correction due to potential (U) was calculated using:

$$\Delta E(U) = \Delta E_0 - neU,$$

where ΔE_0 is the reaction energy at zero potential, n is the number of transferred electrons, and U is the applied potential (referenced to the reversible hydrogen electrode, RHE).

The electrochemically active surface area (ECSA) was estimated from the electrochemical double-layer capacitance (C_{dl}) according to the following equation:

$$\text{ECSA} = C_s / C_d$$

where C_s is the specific capacitance of a smooth electrode surface per unit area. In this work, a commonly adopted value of C_s=40 μF cm^{-2} was used for alkaline aqueous

electrolytes.

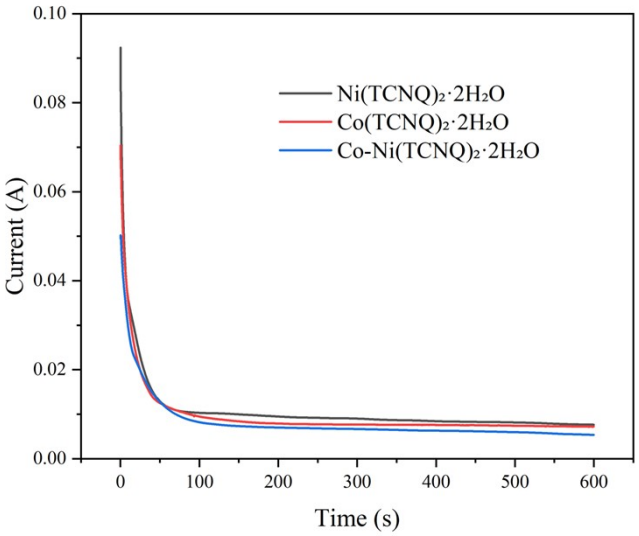

Fig. S1. Chronoamperometric (*i-t*) curves for the electrodeposition of $Ni(TCNQ)_2 \cdot 2H_2O$, $Co(TCNQ)_2 \cdot 2H_2O$, and $Co\text{-}Ni(TCNQ)_2 \cdot 2H_2O$ at 0 V.

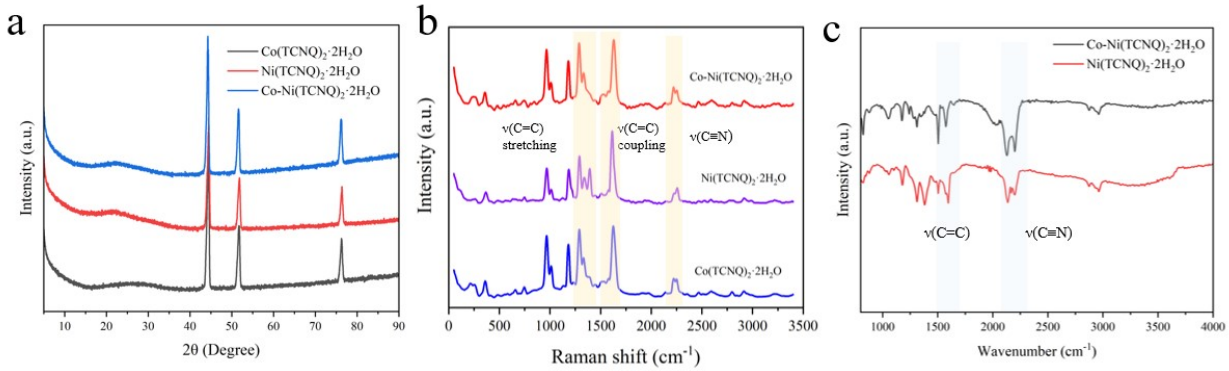

Fig. S2. (a) XRD patterns (b) Raman spectra of $Ni(TCNQ)_2 \cdot 2H_2O$, $Co(TCNQ)_2 \cdot 2H_2O$ and $Co\text{-}Ni(TCNQ)_2 \cdot 2H_2O$, (c) FTIR spectra of $Ni(TCNQ)_2 \cdot 2H_2O$ and $Co\text{-}Ni(TCNQ)_2 \cdot 2H_2O$.

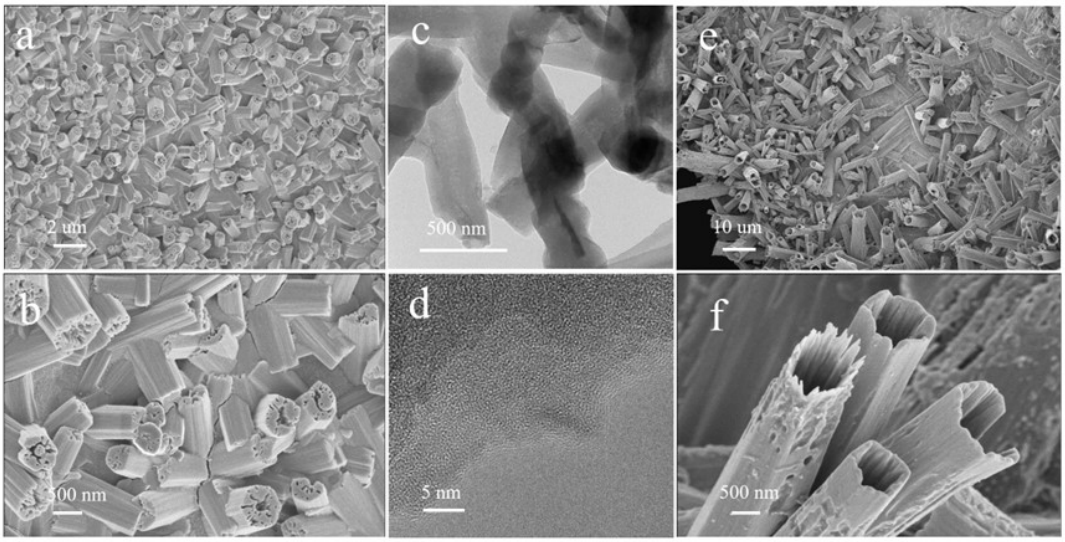

Fig. S3. (a, b) SEM images and (c, d) TEM images of $Ni(TCNQ)_2 \cdot 2H_2O$, and (e, f) SEM images of $Co(TCNQ)_2 \cdot 2H_2O$.

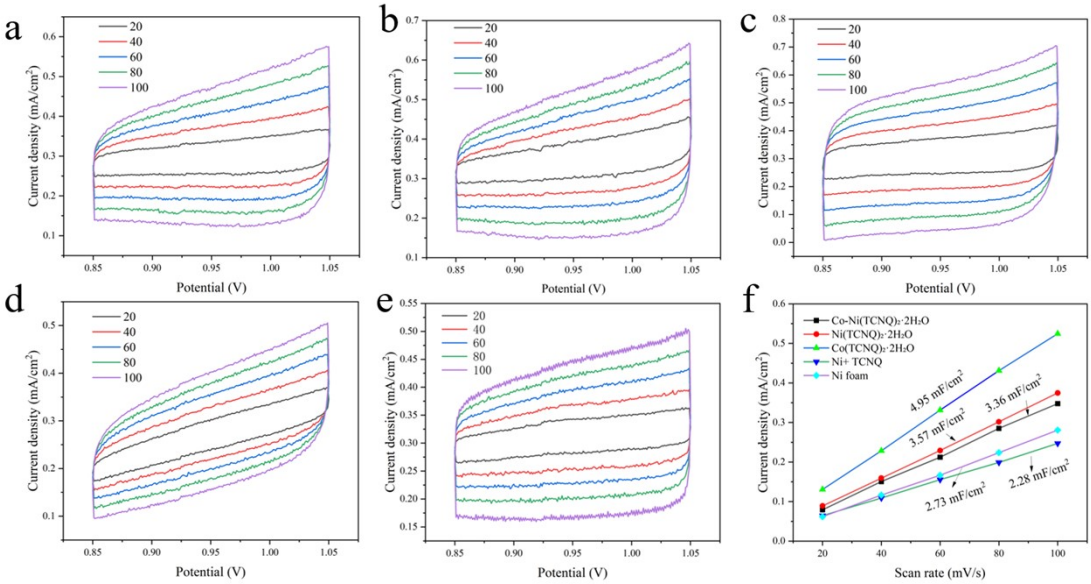

Fig. S4. CV curves of (a) $Co\text{-}Ni(TCNQ)_2 \cdot 2H_2O$, (b) $Ni(TCNQ)_2 \cdot 2H_2O$, (c) $Co(TCNQ)_2 \cdot 2H_2O$, (d) Ni+TCNQ, (e) Ni foam at different scan rates. (c) Estimation of electrochemical active surface area (ECSA) represented by the C_{dl} derived from the CV measurements.

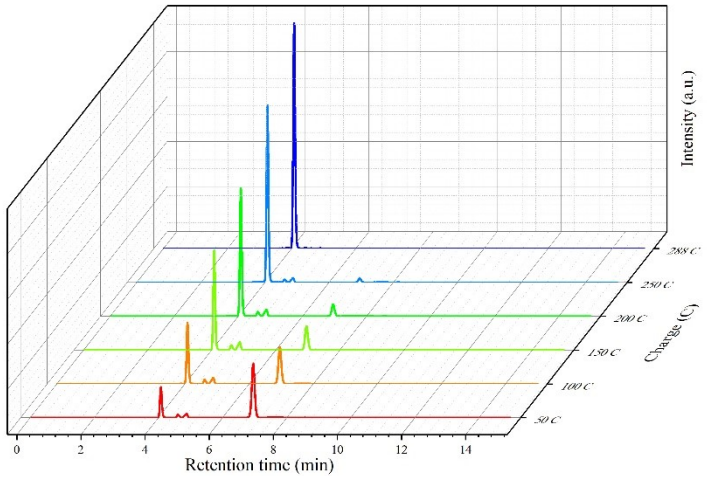

Fig. S5. HPLC chromatograms recorded at different electrolysis charges during HMF oxidation in 1.0 M KOH containing 50 mM HMF.

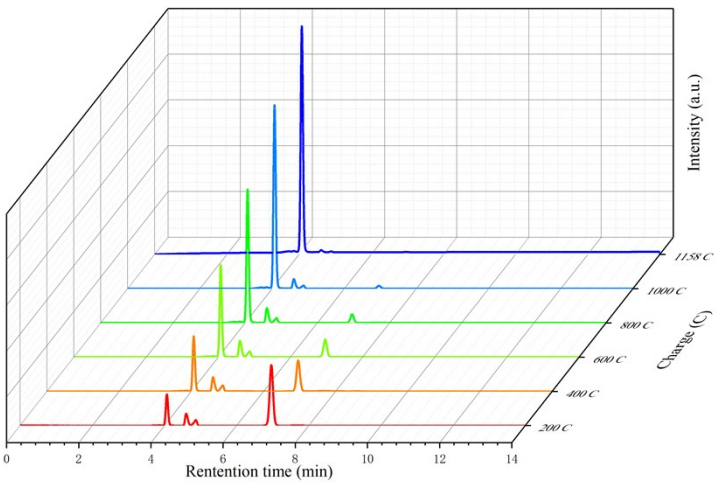

Fig. S6. HPLC chromatograms recorded at different electrolysis charges during HMF oxidation in 1.0 M KOH containing 200 mM HMF.

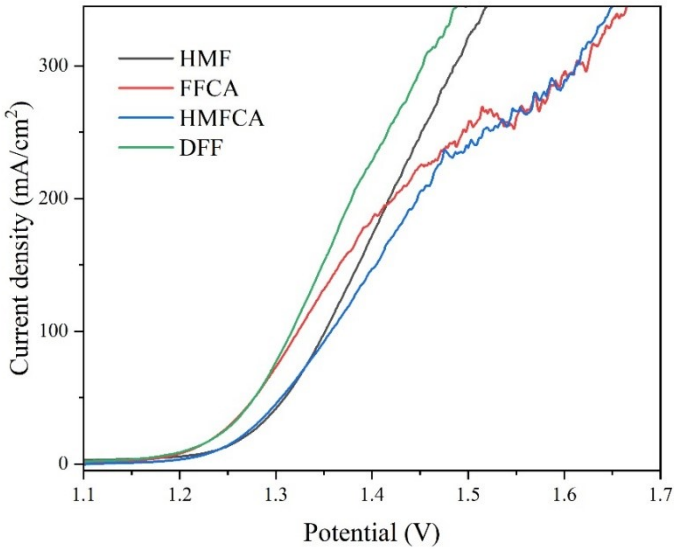

Fig. S7. LSV curves of Co-Ni(TCNQ)$_2$·2H$_2$O in 1.0 M KOH with 50 mM HMF, DFF, FFCA and HMFCA (without *IR* compensation).

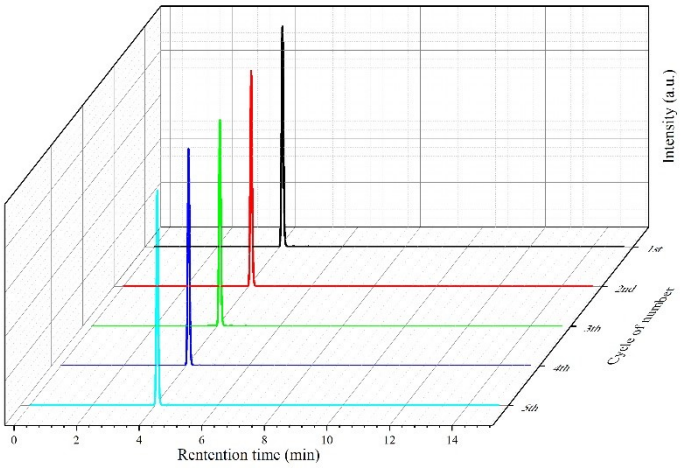

Fig. S8. HPLC chromatograms recorded over successive electrolysis cycles during HMF oxidation in 1.0 M KOH containing 50 mM HMF.

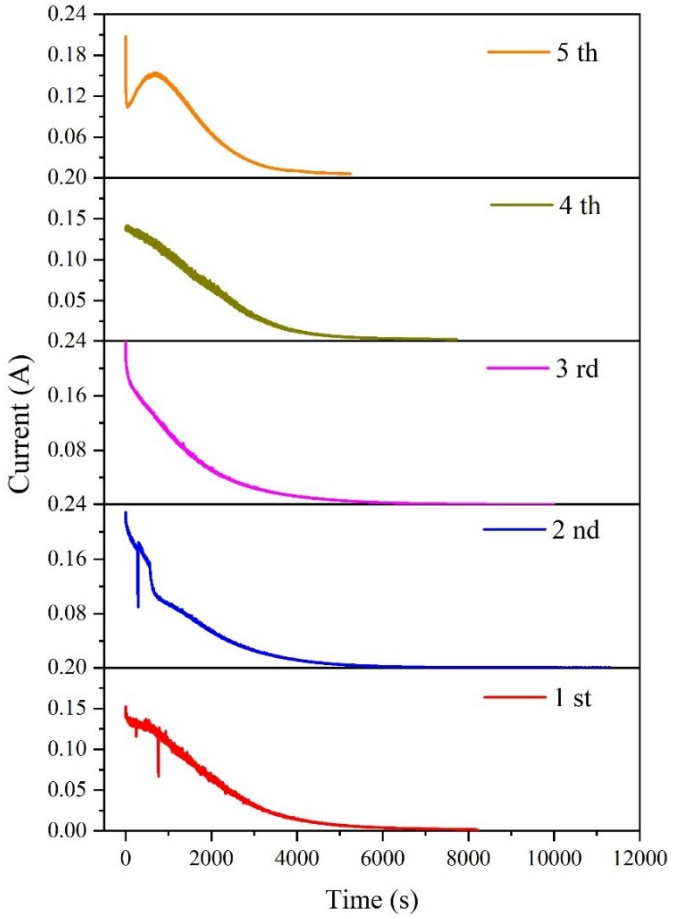

Fig. S9. Current density versus time profile measured over multiple cycles at a constant applied potential of 1.5 V with 50 mM HMF in a H cell. (V=10 ml)

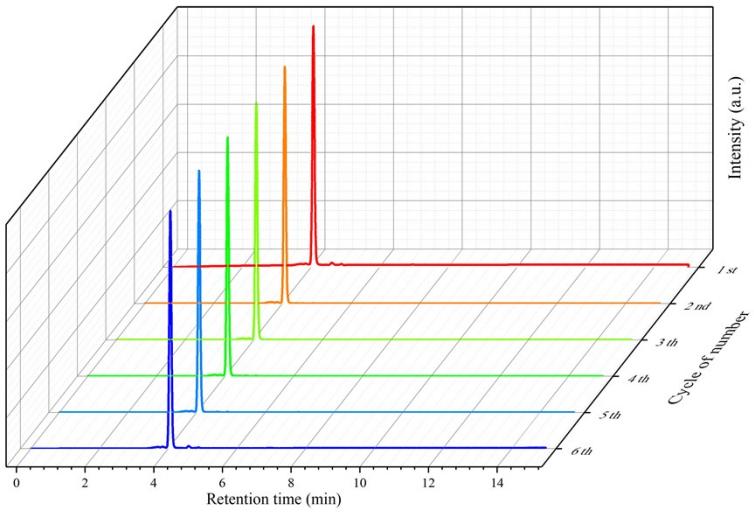

Fig. S10. HPLC chromatograms recorded over successive electrolysis cycles during HMF oxidation in 1.0 M KOH containing 200 mM HMF.

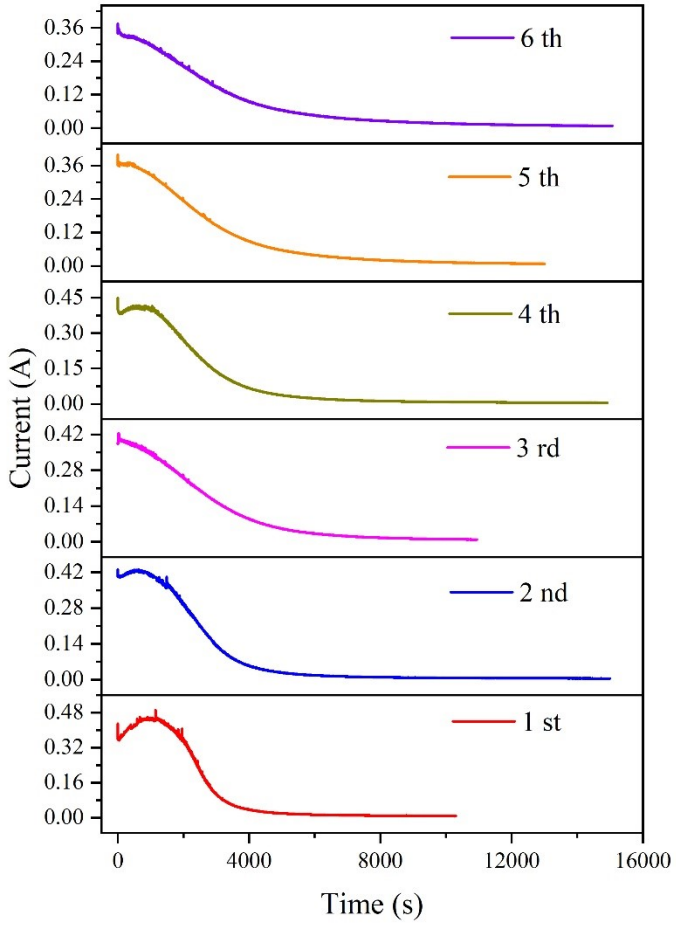

Fig. S11. Current density versus time profile measured over multiple cycles at a constant applied potential of 1.5 V with 200 mM HMF in a H cell (*V*=10 ml).

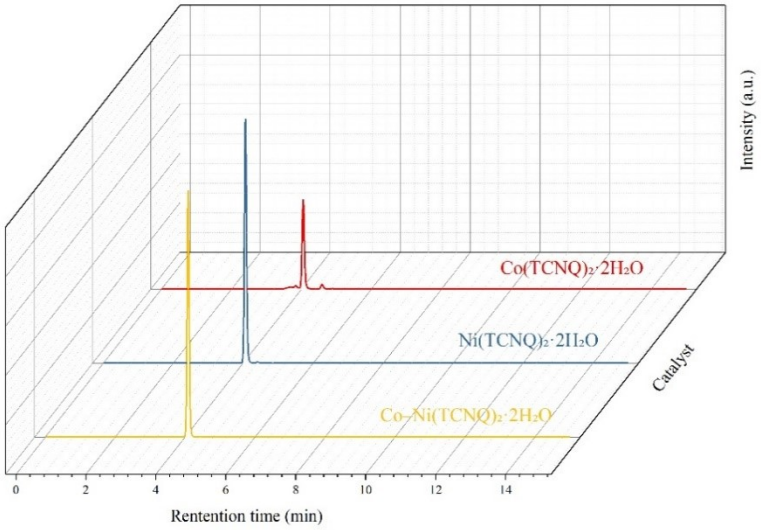

Fig. S12. HPLC chromatograms recorded over different catalysts during HMF oxidation in 1.0 M KOH containing 50 mM HMF in H cell.

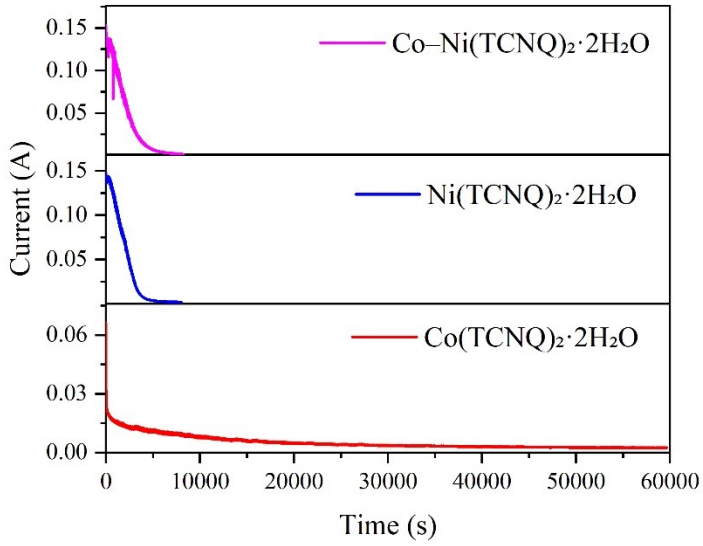

Fig. S13. Current density versus time profile measured over different catalysts at a constant applied potential of 1.5 V with 50 mM HMF in a H cell (V = 10 mL).

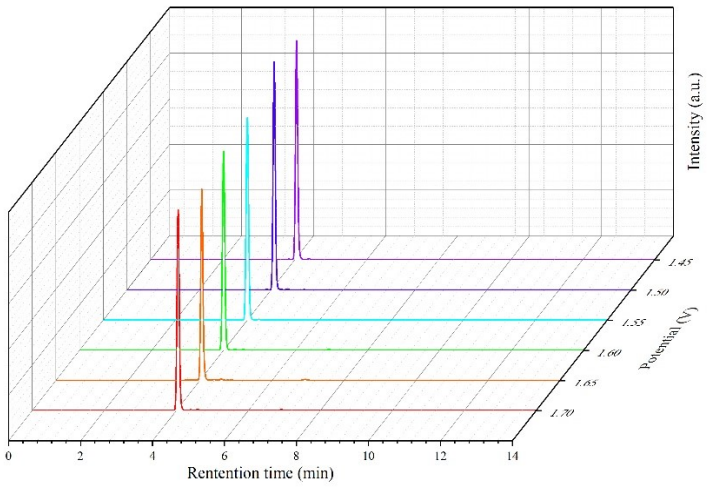

Fig. S14. HPLC chromatograms recorded at different potential with 1.0 M KOH containing 50 mM HMF in H cell.

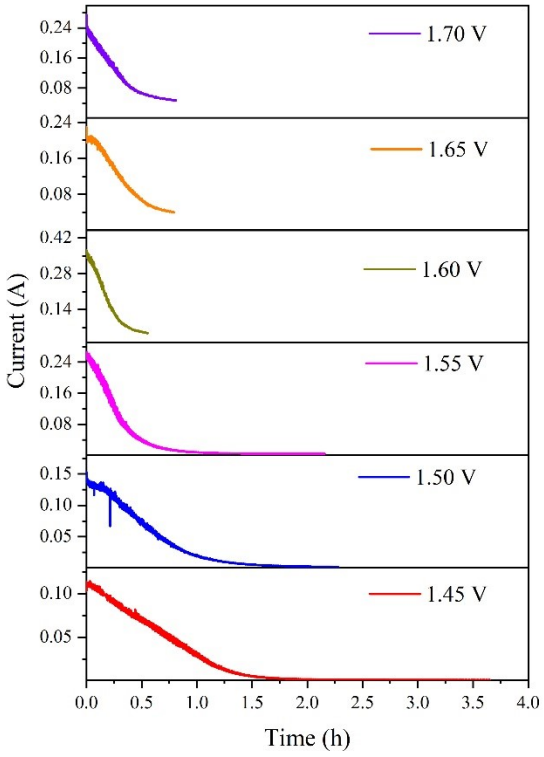

Fig. S15. Current density versus time profile measured at different potential with 50 mM HMF in a H cell (*V*=10 mL, the catalyst area of the 1.65 and 1.70 V is reduced by half due to the upper limit of current).

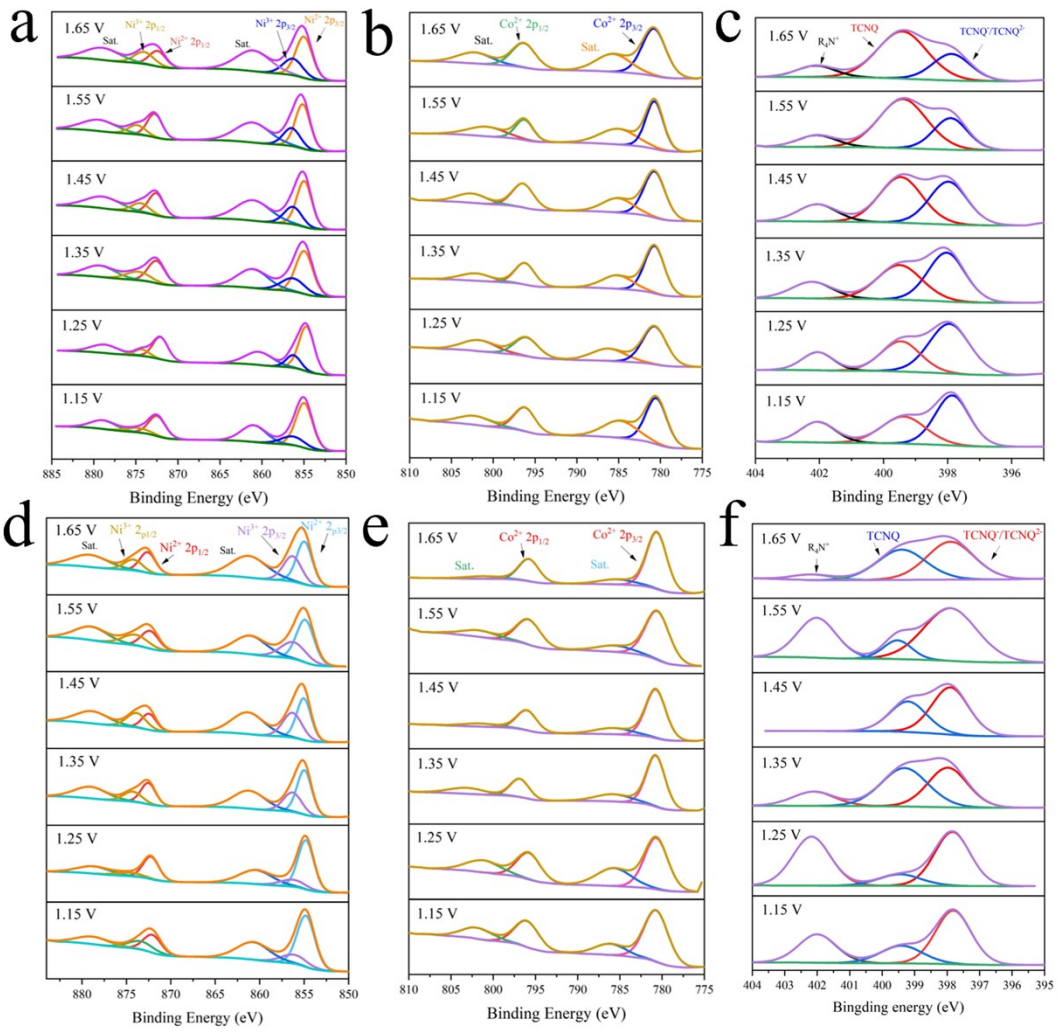

Fig. S16. (a) Ni 2p, (b) Co 2p, and (c) N 1s spectra of Co–Ni(TCNQ)$_2$·2H$_2$O under different applied potentials in 1.0 M KOH containing 200 mM HMF; (d) Ni 2p, (e) Co 2p, and (f) N 1s spectra of Co–Ni(TCNQ)$_2$·2H$_2$O under different applied potentials in 1.0 M KOH without HMF.

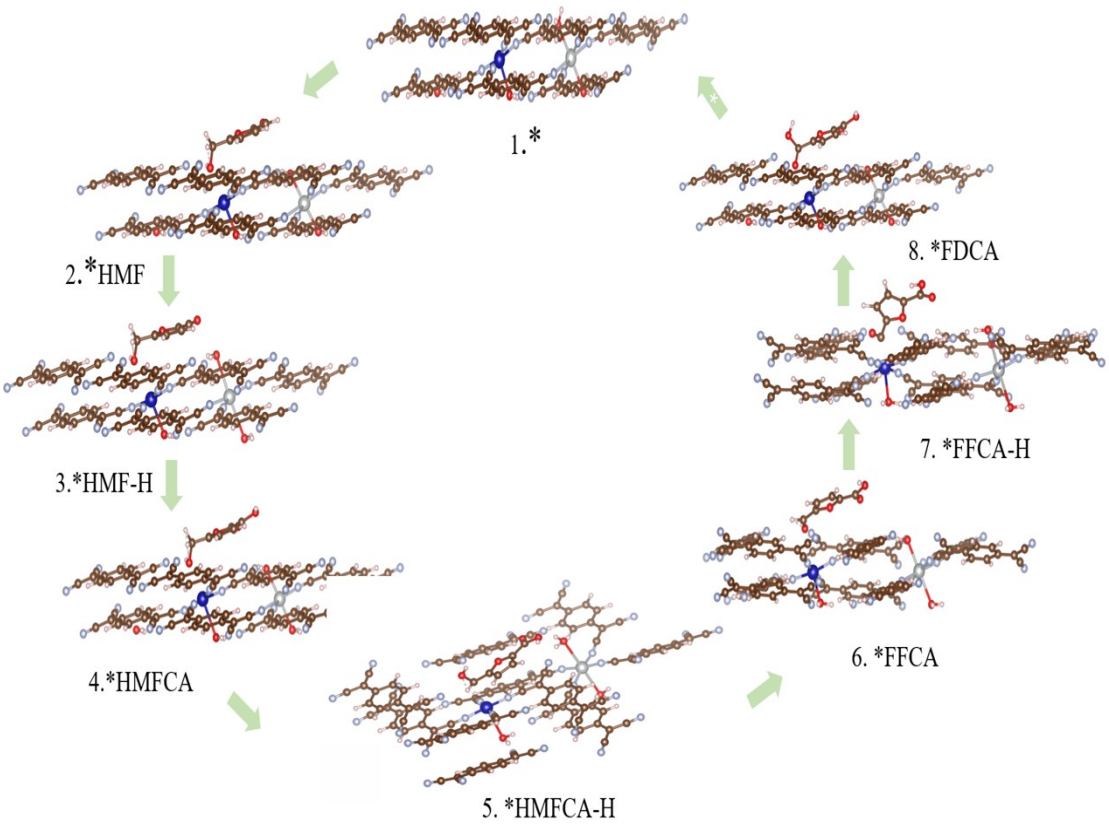

Fig. S17. Optimized adsorption configurations of HMFOR intermediates on the Co–Ni(TCNQ)$_2$·2H$_2$O surface.

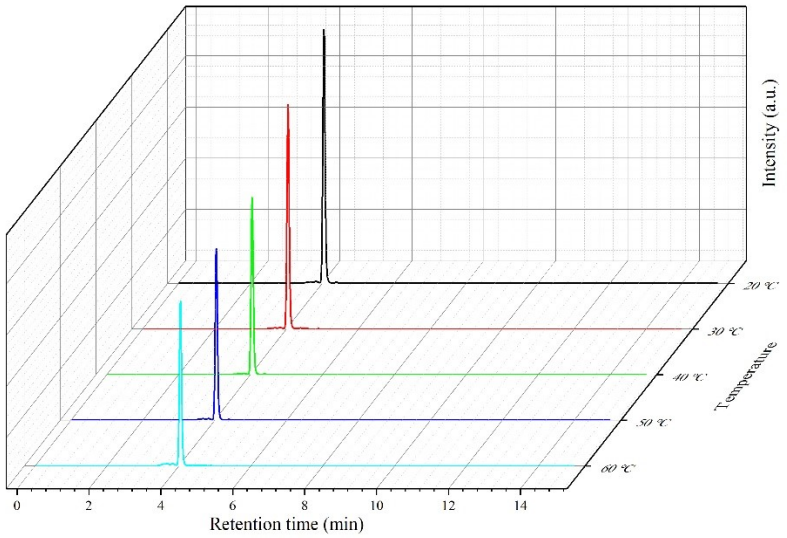

Fig. S18. HPLC chromatograms taken at various cycles at a constant applied potential of 1.8 V in a flow cell.

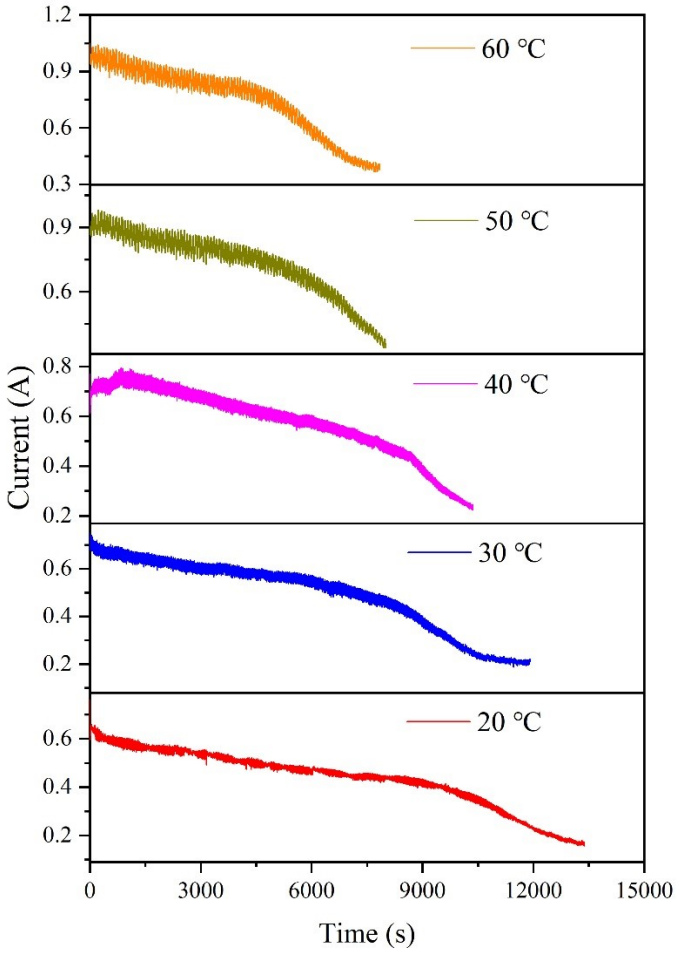

Fig. S19. Chronoamperometry stability test. Current density versus time profile measured over multiple cycles at a constant applied potential of 1.8 V in a flow cell (C_{HMF} = 200 mM, V = 50 mL).

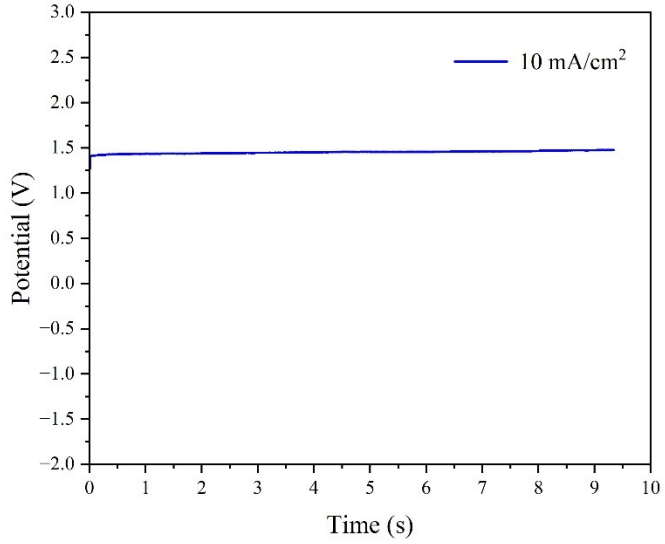

Fig. S20. Chronopotentiometry stability test at a constant current density of 10 mA cm^{-2} in a flow cell (with 1 M HMF).

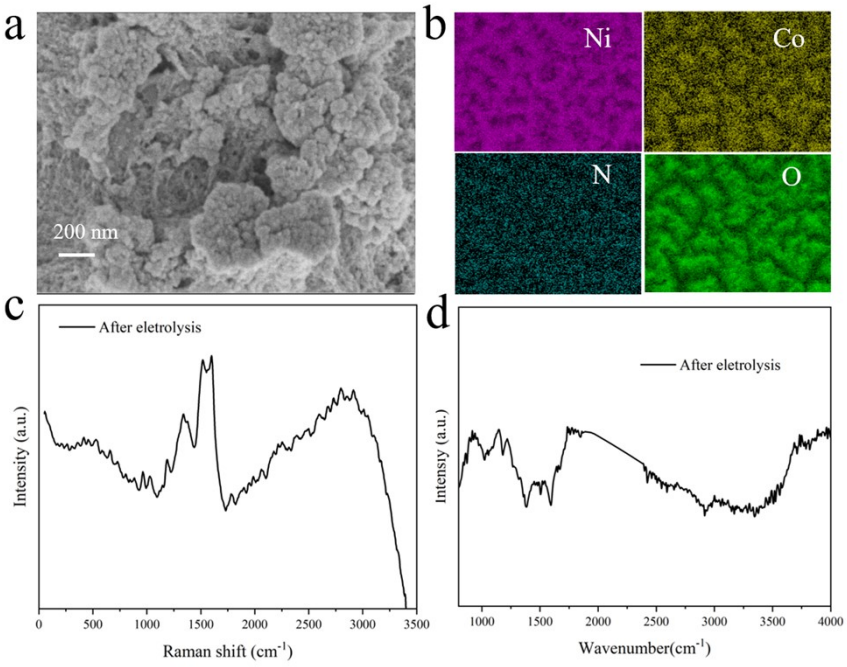

Fig. S21. Post-electrolysis characterization of Co-Ni(TCNQ)$_2$·2H$_2$O electrodes. (a) SEM image of the electrode surface, (b) corresponding elemental mapping, (c) Raman spectra; (d) FTIR spectra.

Table S1. The transferred charge (Q) and the mass loading (Δm) for the chronoamperometric deposition of Ni(TCNQ)$_2$·2H$_2$O, Co(TCNQ)$_2$·2H$_2$O and Co-Ni(TCNQ)$_2$·2H$_2$O catalysts on nickel foam. (The area of nickel foam is 2*3 cm^2)

Catalyst	Initial Mass (g)	Mass after deposition (g)	ΔMass (g)	Charge (C)
Ni(TCNQ)$_2$·2H$_2$O	0.2596	0.2673	0.0077	6.32
Co(TCNQ)$_2$·2H$_2$O	0.2854	0.2952	0.0098	5.65
Co-Ni(TCNQ)$_2$·2H$_2$O	0.2821	0.2921	0.0100	4.88

Table S2. Electrochemical double-layer capacitance and calculated ECSA of different electrodes.

Electrode	C_{dl} (mF·cm^{-2})	ECSA (cm^2)
Co(TCNQ)$_2$·2H$_2$O	4.95	123.8
Ni(TCNQ)$_2$·2H$_2$O	3.57	89.3
Co–Ni(TCNQ)$_2$·2H$_2$O	3.36	84.0
Ni foam	2.73	68.3
Ni + TCNQ	2.28	57.0

Table S3. EIS fitting parameters of Co–Ni(TCNQ)$_2$·2H$_2$O with and without HMF in 1.0 M KOH at

1.35 V.

Solution	With HMF	Without HMF
L_0	189 nH	349 nH
R_0	1.29 Ω	2.03 mΩ
R_1	6.19 Ω	1.98 KΩ
CPE_0 Y_0	51.8 mSs^{α}	354 mSs^{α}
CPE_0 α	646 m	269 m
R_2	32.9 Ω	1.38 KΩ
W	12.2 uDW	68.4 mDW
CPE_0 Y_0	13.5 mSs^{α}	33.7 mSs^{α}
CPE_0 α	912 m	915 m

Reference

[1] J.K. Nørskov, T. Bligaard, J. Rossmeisl, C.H. Christensen, Towards the computational design of solid catalysts, *Nat. Chem.* 1(1) (2009) 37-46.